Metal–Organic Frameworks

DOI: 10.1002/anie.200904983

Freeze Drying Significantly Increases Permanent Porosity and Hydrogen Uptake in 4,4-Connected Metal–Organic Frameworks**

*Liqing Ma, Athena Jin, Zhigang Xie, and Wenbin Lin**

Many potential applications of metal–organic frameworks (MOFs) take advantage of the enormous internal surface areas offered by this emerging class of tunable materials.[1] For example, large permanent porosity has been shown to be key in gas storage,[2] chemical sensing,[3] catalysis,[4] and controlled release of drugs.[5] Although permanent porosity can often be attained by exchanging high boiling-point solvents that are typically in the pores and channels of as-synthesized MOFs with low boiling-point solvents followed by evacuation at elevated temperatures, many MOFs exhibit surface areas that are only a small fraction of what is predicted based on their structures. This problem becomes even more severe for MOFs that are built from elaborately designed organic bridging ligands to impart desirable functions.[6] We have recently developed strategies to enhance permanent porosity in MOFs with varying degrees of success by rigidification of the frameworks with unusual interlocking and interpenetration or by increasing the connectivity of the bridging ligands.[7] Herein we report a simple physical means of achieving high permanent porosity in new 4,4-connected MOFs by freeze drying.

As elegantly demonstrated by Hupp and co-workers, the surface areas of zinc MOFs can be significantly increased by supercritical carbon dioxide (s-CO_2) processing, presumably by preventing the mesopore collapse and thus enhancing micropore accessibility as a result of the low surface tension of s-CO_2.[8] We envisaged that a similar effect can be elicited if the high boiling-point solvents incorporated in the MOFs are exchanged with a solvent (such as benzene) that can be removed by freeze drying. The frozen solvent can be removed from the MOFs by solid–gas transition under vacuum at temperatures below its freezing point. Bypassing the liquid phase eliminates the detrimental effect of surface tension in inducing mesopore collapse, thereby enhancing the permanent porosity of MOFs.

Tetracarboxylic acids with the tetrahedral geometry, methanetetra(*p*-benzoic acid) ($\mathbf{L^1}$-H_4) and methanetetra(biphenyl-*p*-carboxylic acid) ($\mathbf{L^2}$-H_4) were used to synthesize new MOFs in this study.[9] A solvothermal reaction between $\mathbf{L^1}$-H_4 and $Cu(NO_3)_2$ in a diethylformamide (def) and H_2O mixture under acidic conditions afforded blue crystals with a formula of $[Cu_2(\mathbf{L^1})(H_2O)_2]\cdot 6\,def\cdot 2\,H_2O$ (**1**). A similar reaction between $\mathbf{L^2}$-H_4 and $Cu(NO_3)_2$ in a dimethylformamide (dmf)/H_2O mixture yielded blue crystals of $[Cu_2(\mathbf{L^2})(H_2O)_2]\cdot 14\,dmf\cdot 5H_2O$ (**2**; Scheme 1). These formulae were established based on single-crystal X-ray diffraction studies, integration of NMR spectra, and thermogravimetric analysis (TGA) results (Supporting Information).

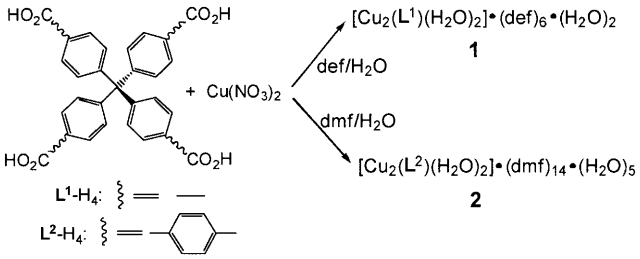

Scheme 1. Preparation of **1** and **2**.

Single-crystal X-ray structure determination of **1** revealed a 3D non-interpenetrating framework that crystallizes in tetragonal space group $P4_2/mmc$.[10] Each asymmetric unit contains one eighth of the ligand $\mathbf{L^1}$, one quarter of a Cu atom, and one quarter of a coordinating H_2O molecule. The Cu atom coordinates to four different carboxylate oxygen atoms of the $\mathbf{L^1}$ ligands in the equatorial positions to form the copper paddle-wheel secondary building units (SBUs). Each unit cell contains two complete ligands $\mathbf{L^1}$ and two Cu paddle-wheels, with H_2O molecules binding to the axial positions, giving the framework formula of $[Cu_2(\mathbf{L^1})(H_2O)_2]$. The tetrahedral ligands (simplified as red tetrahedra in Figure 1 a,b) link the $[Cu_2(O_2CR)_4]$ SBUs to form a 3D framework of the PtS network topology (with the Schläfli symbol $[4^2\cdot 8^4]$).[11] Compound **1** is isostructural to the reported Zn analogue.[12] Compound **1** has open channels along all of the three crystallographic directions, with channel openings of 19.5 × 7.0 Å and 8.4 × 7.0 Å along the *a* and *b* axes (Figure 1 c) and channel openings of 8.4 × 8.4 Å along the *c* axis (Figure 1 d). PLATON calculations[13] of **1** indicated a void volume of 2466 $Å^3$ (72 % of the unit cell volume of 3432 $Å^3$) that is filled with 12 def and 4 water molecules. Consistent with this finding, the TGA analysis of **1** showed a solvent weight loss of 51.5 % in the 20–250 °C temperature range (calcd 52.3 %).

Compound **2** crystallizes in the tetragonal space group $P\bar{4}2_1c$.[10] Compound **2** is isoreticular to compound **1**, with four $\mathbf{L^2}$ ligands and four Cu paddle-wheels in the unit cell. The

[*] Dr. L. Ma, A. Jin, Dr. Z. Xie, Prof. W. Lin
Department of Chemistry, CB#3290, University of North Carolina
Chapel Hill, NC 27599 (USA)
Fax: (+1) 919-962-2388
E-mail: wlin@unc.edu
Homepage: http://www.chem.unc.edu/people/faculty/linw/wlindex.html

[**] We acknowledge financial support from NSF.

Supporting information for this article is available on the WWW under http://dx.doi.org/10.1002/anie.200904983.

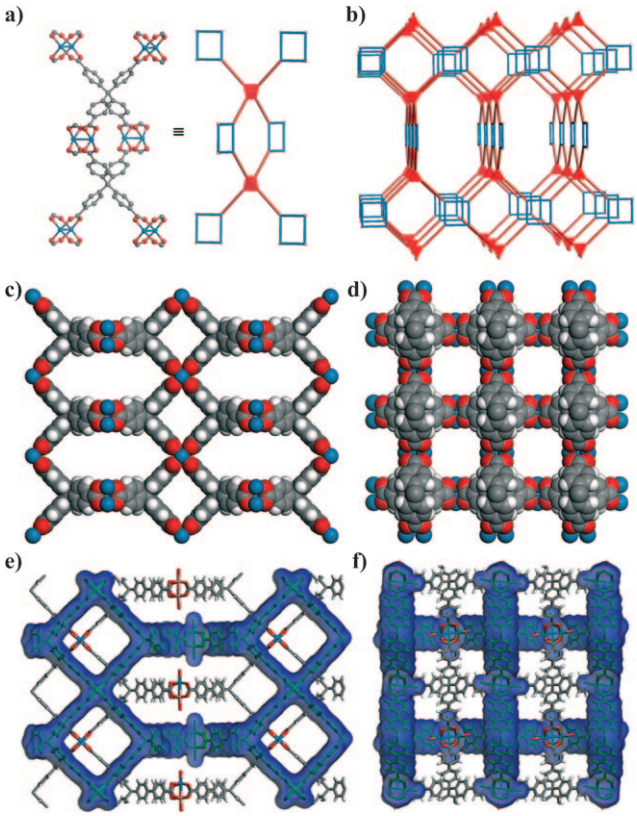

Figure 1. Crystal structures of **1** and **2**. a) Schematic representation of tetracarboxylate ligand $\mathbf{L}^1$ (red tetrahedra) and copper paddle-wheels (blue squares). b) Schematic representation of the 4,4-connected network of the PtS topology for both **1** and **2**. c) Space-filling model of **1** as viewed down the *a* axis (gray C, white H, red O, blue Cu). d) Space-filling model of **1** as viewed down the *c* axis. e) Stick model of twofold interpenetrating networks of **2** as viewed down the *a* axis with one of the networks highlighted in blue. f) Stick model of twofold interpenetrating network of **2** as viewed down the *c* axis with one of the networks highlighted in blue.

axial positions of the $[Cu_2(O_2CR)_4]$ SBUs are terminated with H_2O molecules. Because of the elongated $\mathbf{L}^2$ ligands, compound **2** adopts a twofold interpenetrated PtS network topology (Figure 1e and f). As a result of the twofold interpenetration, compound **2** has smaller open channels of 21.2×3.5 Å and 7.4×7.4 Å along the *a* and *b* axes and of 3.6×3.6 Å along the *c* axis. PLATON calculations[13] of **2** indicated a void volume of 8503 $Å^3$ (73% of the unit cell volume of 11655 $Å^3$) that is filled with 56 def and 20 water molecules. Consistent with this, TGA analysis of **2** showed a solvent weight loss of 54.5% in 20–250 °C temperature range (calcd 55.1%).

We have determined permanent porosity of **1** and **2** by nitrogen adsorption at 77 K, as well as the hydrogen uptake capacity of these porous materials at the same temperature. Both compound **1** and **2** were washed and suspended in methanol (MeOH) overnight, and then washed with dichloromethane (CH_2Cl_2) several times. The resultant solids were then activated at 60 °C under vacuum overnight. The vacuum-dried sample of **1** exhibited a Langmuir surface area of 582 m^2g (a SA_{BET} of 526 m^2g) whereas the vacuum-dried sample of **2** gave a Langmuir surface area of 874 m^2g (a SA_{BET} of 791 m^2g). These values of surface areas are relatively small considering the highly porous nature of these MOFs materials.[14]

We hypothesized that freeze-drying procedures, which are commonly used to dry and preserve delicate biological materials,[15] can be applied to MOF sample pre-treatment for adsorption experiments. In a freeze-drying experiment, the included solvent molecules undergo sublimation (i.e., direct solid→gas conversion without going through the liquid phase). As a result, deleterious effect of solvent surface tension would not be experienced by the MOF framework in the freeze-drying process. After washing with MeOH and CH_2Cl_2, the resultant MOF sample was further washed with benzene several times. The suspension of MOF in benzene was then frozen at 0 °C. After three freeze-thaw cycles, the sample cell was placed under dynamic vacuum in an ice/H_2O bath for 24 h. The ice/H_2O bath was removed and the sample was kept under vacuum at room temperature for another 24 h, and then heated under vacuum at 60 °C for 16 h. As indicated in Figure 2, the adsorption experiments gave much enhanced porosity for the freeze-dried samples. The Langmuir surface increased to 1725 m^2g (with a SA_{BET} of 1560 m^2g) for the freeze-dried sample of **1**, which is a threefold enhancement over the regular vacuum-dried sample. The Langmuir surface of the freeze-dried **2** has increased 29%, to 1127 m^2g (with a SA_{BET} of 1020 m^2g). These freeze-dried MOFs also show a significantly enhanced hydrogen-uptake capacity. For example, H_2 uptake for freeze-dried **1** increased to 1.42 wt%, nearly twice the value of the vacuum-dried sample (0.78 wt%). The H_2 uptake for **2** increased from 1.26 wt% for the vacuum-dried sample to 1.73 wt% for the freeze-dried sample.

Powder X-ray diffraction (PXRD) studies indicated that both compound **1** and **2** retained crystallinity after regular vacuum drying or freeze drying (Figure 3). There is an excellent match between the PXRD patterns of the pristine samples of **1** and **2** with those simulated using their single crystal structures, indicating phase purity for both samples.

The peak positions of vacuum-dried **1** remained unchanged compared to the pristine patterns, but significant peak broadening occurred. This result is consistent with the collapse of larger mesopores during solvent evaporation to lead to much smaller crystalline domains. Interestingly, the PXRD pattern of the freeze-dried **1** is very different from that of the pristine sample, particularly with the emergence of a sharp diffraction peak at a low 2θ of 4.3°. The new PXRD pattern can be reverted to that of the pristine sample by soaking the freeze-dried sample in a def/H_2O mixture. These results are indicative of a breathing phenomenon[16] of **1** during the freeze-drying process. Such a breathing effect is, however, not observed for **1** during the regular vacuum-drying process. The unit cell of freeze-dried **1** can be indexed to give a tetragonal cell of $a' = b' = 22.62(6)$ Å, $c' = 45.30(8)$ Å. The doubling of *a*, *b*, and *c* axes to *a*′, *b*′, and *c*′, is also evidenced by the precession images of the 0*kl* and *k*0*l* planes (Supporting Information). It is noted that the freeze-dried crystal slightly shrinks in the *c* direction from 22.88 Å to 22.65 Å (half the *c*′), and the *a* and *b* directions also shrink from 12.25 Å to 11.31 Å (half of *a*′ or *b*′).

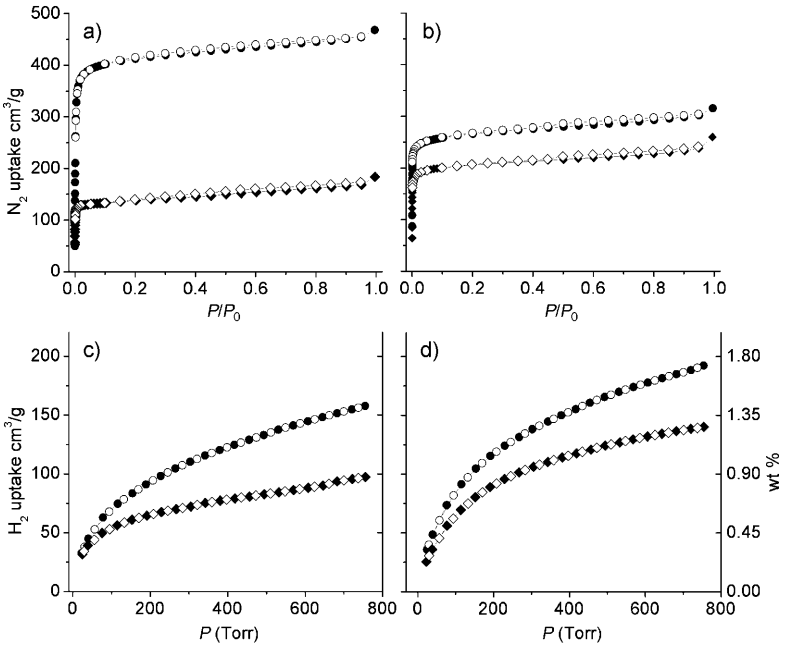

Figure 2. Nitrogen adsorption isotherms of **1** (a) and **2** (b) at 77 K. Hydrogen adsorption isotherms of **1** (c) and **2** (d) at 77 K. Filled symbols: adsorption; empty symbols: desorption. Diamond symbols for vacuum-dried samples; circle symbols for freeze-dried samples.

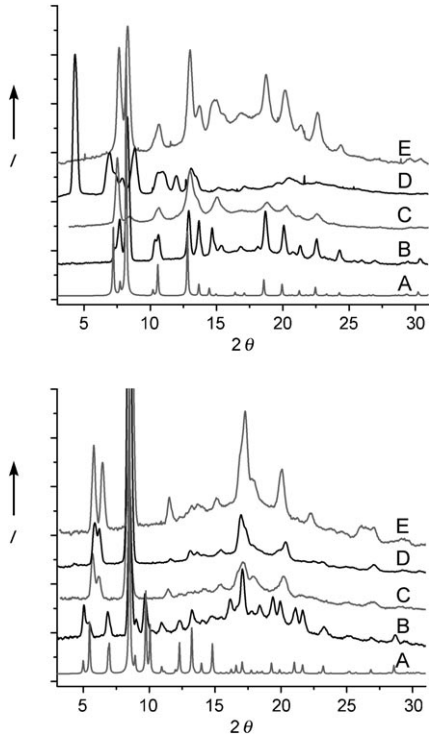

Figure 3. Powder X-ray diffraction (PXRD) patterns of **1** (top) and **2** (bottom). A) simulated from single-crystal structure; B) pristine samples; C) vacuum-dried samples; D) freeze-dried samples; E) freeze-dried samples treated with dmf (or def)/H_2O.

The emergence of a sharp diffraction at 4.3° in freeze-dried **1** also indicates a phase change during the freeze-drying process. A new space group of $I4_1/amd$ can be assigned to the freeze-dried model of **1** (Figure 4a). The first diffraction peak at 4.3° thus results from the (101) Miller plane which is allowed in the $I4_1/amd$ space group. Upon freeze drying, the unit cell volume of **1** changes from 3432 Å^3 to 23178 Å^3.

The PXRD patterns for compound **2** after vacuum drying and freeze drying appear to be the same but both different from that of the pristine sample. Peak indexing[17] of **2** also indicated a breathing effect, resulting in a new tetragonal unit cell with $a = 21.511$ and $c = 28.628$ Å. The c axis thus shrinks from 35.410 to 28.628 Å whereas the a and b axes have expanded from 18.143 to 21.511 Å. The strong diffraction at $2\theta = 8.5°$ is assigned to the (112) plane. The large peak width at $2\theta = 8.5°$ is a result of the overlapping of the (112) plane with two other strong diffractions of (200) and (201) which are expected to appear at 2θ of 8.2° and 8.8°, respectively. In the freeze-dried model of **2**, the two interpenetrating networks have moved towards each other with the copper paddle-wheels lined up in a co-planar orientation (* in Figure 4b). The resulting network has the space group $P4_2/nmc$, which has higher symmetry than the original $P\bar{4}2_1/c$. Upon freeze drying, the unit cell volume of **2** has changed from 11656 Å^3 to 13247 Å^3.

The PXRD patterns of the vacuum-dried, freeze-dried, and solvent-treated freeze-dried samples of **2** all show similar peak positions, but different from the PXRD pattern of pristine **2**. The irreversible change of the PXRD patterns upon regular vacuum drying or freeze drying of **2** can be

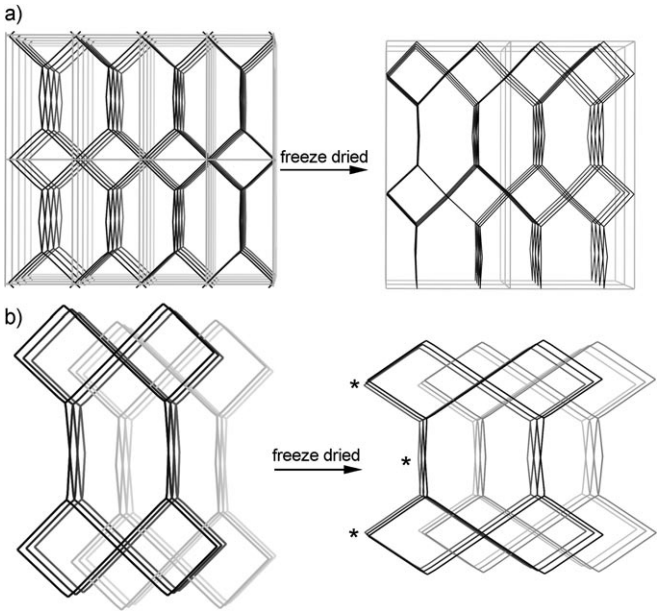

Figure 4. Schematic representation of the freeze-dried model of a) **1**, all of the cell axes doubled, transforming to a body-centered cell; and b) **2**, the cell shrinks along the c direction while expanding along the a and b directions. * indicates co-planer copper paddle-wheels.

attributed to the doubly interpenetrating nature of **2**. When the included solvents are removed from the crystal channels, the two networks move toward each other, presumably leading to a more stable structure with attractive interactions between the two frameworks. As a result, the solvent molecules can only refill the void space generated during the drying process.

In summary, we have applied an old technique to enhance the properties of a new class of materials. By freeze drying MOFs, especially ones containing elongated ligands and with very large channels, we have preserved their structures better and enhanced their porosity and hydrogen uptake. We believe that the freeze-drying method will be widely applied to pretreat many porous materials, including MOFs, for a number of applications in the future owing to the ease and simplicity of freeze-drying procedures.

Experimental Section

1: A mixture of $\mathbf{L}^1$-H_4 (15 mg, 0.030 mmol) and $Cu(NO_3)_2{\cdot}2.5\,H_2O$ (30 mg, 0.13 mmol) in def/H_2O (4.5 mL/1.5 mL) mixed solvents was placed in a screw-capped vial. After addition of several drops of HCl (3 M, aq.), the vial was capped and placed in an oven at 80 °C for one day. Blue crystals of **1** were collected by filtration (27.6 mg, 72%). Solvent content calcd (%) from the proposed formula: def: 46.7, H_2O: 5.5; determined by ^{1}H-NMR/TGA: def: 46.4, H_2O 5.1. Compound **2** was similarly synthesized.

Typical freeze-drying procedure: After decanting all the mother liquid, freshly prepared crystals of **1** (ca. 30 mg) were washed with MeOH three times over a 12 h period, and then washed with CH_2Cl_2 three times. The resulting dark blue crystals were washed with benzene several times and then soaked in benzene overnight before loading into a BET sample cell. About 1 mL of benzene was left in the sample cell, and the sample cell was then frozen at 0 °C. After three freeze-thaw cycles, the sample cell was placed in an ice/H_2O bath and evacuated under a dynamic vacuum for 24 h. The ice/H_2O bath was removed and the sample was kept under vacuum at room temperature for another 24 h, and then heated under vacuum at 60 °C for 16 h. The resulting freeze-dried **1** (14.1 mg) was used to perform gas-uptake measurements. N_2 uptake measurements were carried out at $P/P_o = 8\times10^{-6}$ to 0.995, H_2 uptake measurements were carried out in the 0.03 to 1.0 atm range.

Received: September 5, 2009
Published online: November 19, 2009

Keywords: freeze drying · gas storage · hydrogen storage · metal–organic frameworks · porous materials

[1] a) M. Eddaoudi, J. Kim, N. Rosi, D. Vodak, J. Wachter, M. O'Keeffe, O. M. Yaghi, *Science* **2002**, *295*, 469; b) O. R. Evans, W. Lin, *Acc. Chem. Res.* **2002**, *35*, 511 – 522; c) G. Férey, C. Mellot-Draznieks, C. Serre, F. Millange, *Acc. Chem. Res.* **2005**, *38*, 217.

[2] a) J. L. C. Rowsell, O. M. Yaghi, *Angew. Chem.* **2005**, *117*, 4748 – 4758; *Angew. Chem. Int. Ed.* **2005**, *44*, 4670 – 4679; b) M. Dincă, J. R. Long, *Angew. Chem.* **2008**, *120*, 6870 – 6884; *Angew. Chem. Int. Ed.* **2008**, *47*, 6766 – 6779; c) B. Kesanli, Y. Cui, M. Smith, E. Bittner, B. Bockrath, W. Lin, *Angew. Chem.* **2005**, *117*, 74 – 77; *Angew. Chem. Int. Ed.* **2005**, *44*, 72 – 75.

[3] a) B. Chen, L. Wang, Y. Xiao, F. R. Fronczek, M. Xue, Y. Cui, G. Qian, *Angew. Chem.* **2009**, *121*, 508 – 511; *Angew. Chem. Int. Ed.* **2009**, *48*, 500 – 503; b) M. D. Allendorf, R. J. T. Houk, L. Andruszkiewicz, A. A. Talin, J. Pikarsky, A. Choudhury, K. A. Gall, P. J. Hesketh, *J. Am. Chem. Soc.* **2008**, *130*, 14404 – 14405; c) A. Lan, K. Li, H. Wu, D. H. Olsson, T. J. Emge, W. Ki, M. Hong, J. Li, *Angew. Chem.* **2009**, *121*, 2370 – 2374; *Angew. Chem. Int. Ed.* **2009**, *48*, 2334 – 2338.

[4] a) L. Ma, C. Abney, W. Lin, *Chem. Soc. Rev.* **2009**, *38*, 1248 – 1256; b) J. Lee, O. K. Farha, J. Roberts, K. A. Scheidt, S. T. Nguyen, J. T. Hupp, *Chem. Soc. Rev.* **2009**, *38*, 1450 – 1459.

[5] a) P. Horcajada, C. Serre, M. Vallet-Regí, M. Sebban, F. Taulelle, G. Férey, *Angew. Chem.* **2006**, *118*, 6120 – 6124; *Angew. Chem. Int. Ed.* **2006**, *45*, 5974 – 5978; b) P. Horcajada, C. Serre, G. Maurin, N. A. Ramsahye, F. Balas, M. Vallet-Regí, M. Sebban, T. Taulelle, G. Férey, *J. Am. Chem. Soc.* **2008**, *130*, 6774 – 6780.

[6] a) X. Lin, J. H. Jia, X. B. Zhao, K. M. Thomas, A. J. Blake, G. S. Walker, N. R. Champness, P. Hubberstey, M. Schröder, *Angew. Chem.* **2006**, *118*, 7518 – 7524; *Angew. Chem. Int. Ed.* **2006**, *45*, 7358 – 7364; b) L. Ma, W. Lin, *J. Am. Chem. Soc.* **2008**, *130*, 13834 – 13835; c) L. Ma, J. Lee, J. Li, W. Lin, *Inorg. Chem.* **2008**, *47*, 3955 – 3957; d) X. Lin, I. Telepeni, A. J. Blake, A. Dailly, C. M. Brown, J. M. Simmons, M. Zoppi, G. S. Walker, K. M. Thomas, T. J. Mays, P. Hubberstey, N. R. Champness, M. Schröder, *J. Am. Chem. Soc.* **2009**, *131*, 2159 – 2171.

[7] a) L. Ma, D. J. Mihalcik, W. Lin, *J. Am. Chem. Soc.* **2009**, *131*, 4610 – 4612; b) L. Ma, W. Lin, *Angew. Chem.* **2009**, *121*, 3691 – 3694; *Angew. Chem. Int. Ed.* **2009**, *48*, 3637 – 3640.

[8] A. P. Nelson, O. K. Farha, K. L. Mulfort, J. T. Hupp, *J. Am. Chem. Soc.* **2009**, *131*, 458 – 460.

[9] 1,1′,1″,1‴-Methanetetra(biphenyl-*p*-carboxylic acid) ($\mathbf{L}^2$-H_4) was synthesized by a Pd-catalyzed Suzuki coupling between tetrakis(4-bromophenyl)methane and 4-(methoxycarbonyl)phenylboronic acid followed by a base-catalyzed hydrolysis reaction (Supporting Information).

[10] Single-crystal X-ray diffraction data were measured on a Bruker SMART Apex II CCD-based X-ray diffractometer system equipped with a Cu-target X-ray tube ($\lambda = 1.54178$ Å). Crystal data for **1**: Tetragonal, space group: $P4_2/mmc$, $a = 12.2480(9)$, $c = 22.8767(17)$ Å, $V = 3431.8(4)$ Å^3, $Z = 4$, $\rho_{calcd} = 0.630$ g cm^{-3}, $\mu(Cu_{K\alpha}) = 0.967$ mm^{-1}, Data/restrains/parameters: 759/0/56, $R1(I>2\sigma(I)) = 0.0612$, $wR2 = 0.1785$, R1(all data) = 0.0659, $wR2$(all data) = 0.1816, GOF = 1.073. Crystal data for **2**: Tetragonal, space group: $P\bar{4}2_1c$, $a = 18.1427(6)$, $c = 35.410(2)$ Å, $V = 11655.4(10)$ Å^3, $Z = 4$, $\rho_{calcd} = 0.545$ g cm^{-3}, $\mu(Cu_{K\alpha}) = 0.644$ mm^{-1}, Data/restrains/parameters: 2326/150/244, $R1(I>2\sigma(I)) = 0.0635$, $wR2 = 0.1388$, $R1$(all data) = 0.1179, $wR2$(all data) = 0.1575, GOF = 0.869 (0.868, restrained). CCDC 739240 and CCDC 739241 contain the supplementary crystallographic data for this paper. These data can be obtained free of charge from The Cambridge Crystallographic Data Centre via www.ccdc.cam.ac.uk/data_request/cif.

[11] V. A. Blatov, A. P. Shevchenko, V. N. Serezhkin, *Russ. J. Coord. Chem.* **1999**, *25*, 453 – 465; http://www.topos.ssu.samara.ru.

[12] J. Kim, B. Chen, T. M. Reineke, H. Li, M. Eddaoudi, D. B. Moler, M. O'Keeffe, O. M. Yaghi, *J. Am. Chem. Soc.* **2001**, *123*, 8239 – 8247.

[13] A. L. Spek, *J. Appl. Crystallogr.* **2003**, *36*, 7 – 13.

[14] Grand Canonical Monte Carlo (GCMC) simulation of N_2 adsorption isotherms shows Langmuir surface areas of 3166 m^2 g^{-1} and 3654 m^2 g^{-1} for **1** and **2**, respectively (Supporting Information).

[15] L. Rey, *Nature* **1990**, *345*, 185 – 186.

[16] a) C. Serre, F. Millange, C. Thouvenot, M. Noguès, G. Marsolier, D. Louër, G. Férey, *J. Am. Chem. Soc.* **2002**, *124*, 13519 – 13526; b) P. L. Llewellyn, G. Maurin, T. Devic, S. Loera-Serna, N. Rosenbach, C. Serre, S. Bourrelly, P. Horcajada, Y. Filinchuk, G. Férey, *J. Am. Chem. Soc.* **2008**, *130*, 12808 – 12814.

[17] T. Roisnel, J. Rodriguez-Carvajal, WinPLOTR [ver. May 2009].

